Journal of Zhejiang University-SCIENCE A (Applied Physics & Engineering)
ISSN 1673-565X (Print); ISSN 1862-1775 (Online)
www.jzus.zju.edu.cn; www.springerlink.com
E-mail: jzus@zju.edu.cn

Enhanced compressive performance of concrete via 3D-printing reinforcement*

Li-feng FAN[1], Li-juan WANG[1], Guo-wei MA[2], Peng-fei LI[†‡1], Ming-jie XIA[1]

[1]*College of Architecture and Civil Engineering, Beijing University of Technology, Beijing 100124, China*

[2]*School of Civil and Transportation Engineering, Hebei University of Technology, Tianjin 300401, China*

[†]E-mail: lpf@bjut.edu.cn

Received Apr. 1, 2019; Revision accepted July 30, 2019; Crosschecked Aug. 6, 2019

Abstract: Carbon-nanotube shaped reinforcement (CSR) and traditional latitude and longitude reinforcement (LLR) made of tough resin were 3D printed and applied to concrete specimens. The element numbers of 10, 12, and 14 per layer were selected to investigate the reinforcement by CSR and LLR separately. The uniaxial compressive behaviors of the CSR and LLR reinforced concrete specimens were studied by a series of laboratory tests. The experimental results indicate that the strength of a CSR reinforced specimen with 10, 12, and 14 elements per layer increases by 59.77%, 85.94%, and 108.98%, respectively, compared with the unreinforced specimen. The strength of the LLR reinforced specimen with 10, 12, and 14 elements per layer increases by 24.22%, 46.88%, and 68.75%, respectively, compared with the unreinforced specimen. CSR thus demonstrates higher efficiency in compressive strength improvement than LLR does. The results also show that the failure pattern changes from global failure to partial failure as the element number per layer of CSR increases. The present research provides a potential innovative reinforcing technology for civil engineering applications.

Key words: 3D-printing; Carbon-nanotube shaped reinforcement (CSR); Latitude and longitude reinforcement (LLR); Reinforced concrete

https://doi.org/10.1631/jzus.A1900135 **CLC number:** TU502.6

1 Introduction

Concrete is widely used in building and infrastructure construction. Based on the mature theory framework, researchers have gained the insight into the nature of the 3D mechanical behavior of concrete (Wang et al., 2018; Lu et al., 2019). However, its engineering performance is limited by its low ductility and its brittle charactistics, which may result in structure collapse (Micelli and Nanni, 2004; Dias and Thaumaturgo, 2005; Pendhari et al., 2008; Ahmed and Maalej, 2009; Chi et al., 2014). Therefore, an innovative reinforcing technique is of significance for civil engineering (Wight et al., 2001; Micelli and Nanni, 2004; Dias and Thaumaturgo, 2005; Ouyang et al., 2006; Jiang et al., 2008; Pendhari et al., 2008; Tsonos, 2008; Ahmed and Maalej, 2009; Zhang and Zhu, 2010; Jiang and Fan, 2013, 2015; Chi et al., 2014; Lin et al., 2014; Carballosa et al., 2015; Chen et al., 2015; Chuah et al., 2016).

Currently, latitude and longitude reinforcement (LLR) is generally used because of its easy operation and low cost. However, it is released that the rectangular shape of the element formed in LLR is not the perfect shape for uniformly distributing stress in the concrete. Research has been conducted to investigate the effects of element shape on the reduction of stress concentration. It has been found that the carbon-nanotube with a hexagonal element shape has

‡ Corresponding author

* Project supported by the National Natural Science Foundation of China (No. 51627812)

ORCID: Li-feng FAN, https://orcid.org/0000-0002-7744-692X; Peng-fei LI, https://orcid.org/0000-0002-4996-368X

excellent characteristics, such as large compressive strength and low stress concentration (Treacy et al., 1996; Lee et al., 1997; Wong et al., 1997; Ajayan, 1999; Salvetat et al., 1999). However, the proper utilization of carbon-nanotube shaped elements in force dispersion, stress concentration reduction, and loading capacity improvement for concrete reinforcement has been limited by construction technology.

Recently, the rapid development of 3D-printing technology provides a potential approach for concrete reinforcement. 3D-printing technology is an emerging technology in the manufacturing field, and has been identified as an industrial revolution (Walters and Davies, 2010). It has the advantages of high precision, fast production, and saving of materials with almost no left-over waste. It has been successfully applied in the fields of medicine (Michalski and Ross, 2014) and process manufacture (Sanz-Izquierdo and Parker, 2013) as well as in construction engineering (Pegna, 1997; Le et al., 2012; Cesaretti et al., 2014). In addition, 3D-printing technology provides a flexible way to produce arbitrary forms of reinforcement element, such as carbon-nanotube shaped reinforcement (CSR). Although the application of 3D-printing technology has great potential in concrete reinforcement engineering, its influence on design parameters, such as the element shape and reinforcement ratio, and the improvement of low-ductile and brittle characteristics by such reinforcement have not yet been explored.

In this study, CSR is introduced by the 3D-printing technology. Its improvement of the compressive performance of concrete is compared with the traditional LLR concrete by a series of compression tests. The optimal reinforcement ratio is proposed and the modified fail pattern is discussed to show the advantages of CSR.

2 Experimental program

2.1 Material properties

The present study aims to investigate the effects of the geometrical parameters of the reinforcement element, in which materials which have similar behaviors to steel are generally used. In the present study, a 3D-printing photopolymer was utilized to produce a durable and accurate 3D reinforcement element. The material has a white, opaque appearance with performance comparable with acrylonitrile-butadiene-styrene (ABS). Tension and compression tests were performed to obtain its mechanical properties.

Fig. 1 shows the typical tensile and compressive results. It is seen from Fig. 1 that the 3D-printing material shows a stable performance for both compressive and tensile behaviors. Moreover, its stress-strain curves are similar to those of traditional metallic reinforcing materials. Therefore, a reduced scale model was designed to study the effects of element shape on the reinforcement of concrete as shown in Fig. 2.

It is also noted that the strengths of the concrete and the reinforcing material should be matched to achieve the best performance in practical engineering. Therefore, cement mortar with strength of M2.5 was adopted as the filling material according to the code for design of concrete structures (MOHURD, 2010a).

In addition, the reinforcement ratio in concrete should be controlled within a reasonable range. Too

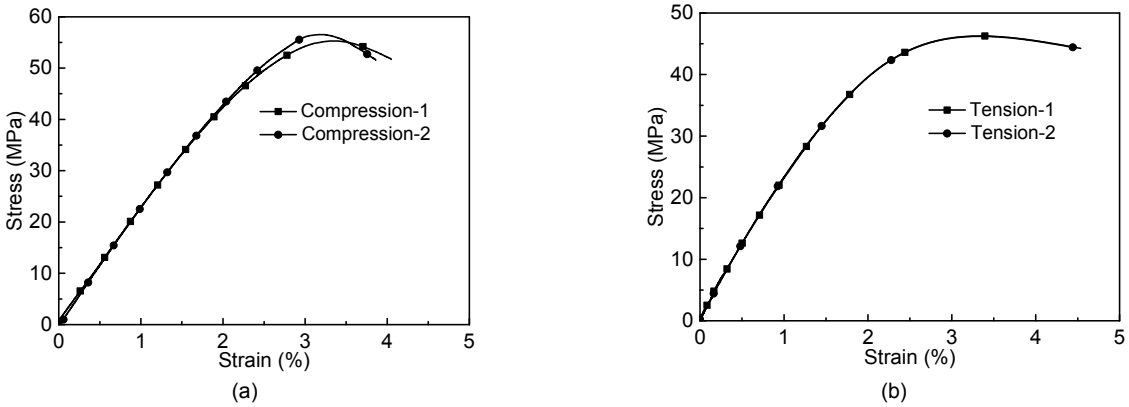

Fig. 1 Mechanical behavior of 3D-printing material
(a) Compressive behavior; (b) Tensile behavior

small a reinforcement ratio leads to brittle failure while too large a reinforcement ratio leads to material waste. In the present study, 10, 12, and 14 elements per layer were specified for the reinforcement as shown in Fig. 2. C10, C12, and C14 denote that the concrete was reinforced by CSR with 10, 12, and 14 elements per layer, respectively. P10, P12, and P14 denote that the concrete was reinforced by LLR with 10, 12, and 14 elements per layer, respectively. The reinforcing cage has a diameter of 90 mm and a length of 190 mm.

To eliminate the influence of random environmental factors on the experimental results, three specimens were made for each of the six types of reinforcements (Fan et al., 2017). For comparison, three concrete specimens without reinforcement were also tested to demonstrate the effects of reinforcement. All the specimens, as shown in Table 1, were approximately 200 mm in height and 100 mm in diameter (MOC, 2003; Wu et al., 2010a, 2010b).

2.2 Sample production

Digital models of carbon nanotube reinforcement and traditional reinforcement were built up as shown in Fig. 2. Using the 3D-printing material, two types of designed reinforcement were printed by an SLA600-3D printer with laser curing 3D-printing technology as shown in Figs. 2a and 2b, respectively.

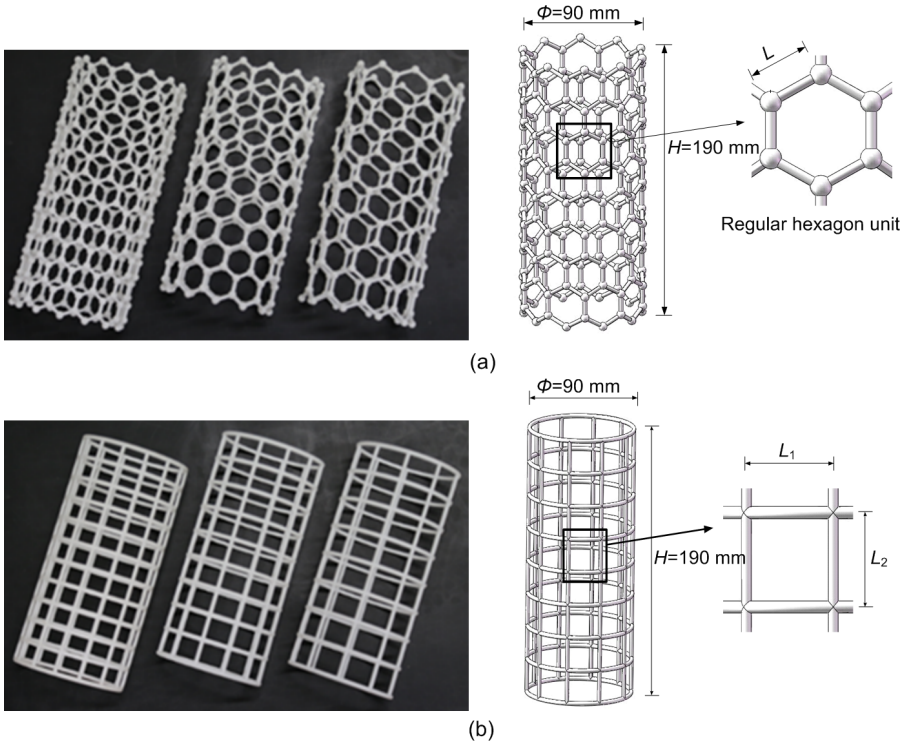

Fig. 2 Two types of reinforcement structures by 3D-printing

(a) Carbon-nanotube shaped reinforcement (CSR); (b) Traditional latitude and longitude reinforcement (LLR). The description of the variables is shown in Tables 2 and 3

Table 1 Experimental samples

Reinforcement type	Reinforcement density	Sample
No reinforcement	0 element (N)	N-1, N-2, N-3
CSR	10 elements (C10)	C10-1, C10-2, C10-3
	12 elements (C12)	C12-1, C12-2, C12-3
	14 elements (C14)	C14-1, C14-2, C14-3
LLR	10 elements (P10)	P10-1, P10-2, P10-3
	12 elements (P12)	P12-1, P12-2, P12-3
	14 elements (P14)	P14-1, P14-2, P14-3

Tables 2 and 3 show the parameters for the reinforcement. According to the specifications for the mix proportion design of masonry mortar (MOHURD, 2010b), the quantity ratios of cement, medium sand, and water were given as 200 kg/m^3, 1450 kg/m^3, and 320 kg/m^3, respectively. After mixing, concrete was placed into the molds via the 3D-printing reinforcements and vibrated. The samples were cured in a standard concrete curing box. Twenty-four hours later, the molds were removed and the specimens were cured for 28 d in a standard curing box.

3 Results and discussion

3.1 Stress-strain relationship

From the uniaxial compression tests, the compressive stress-strain curves of each specimen were obtained. The stress-strain curves of samples without reinforcement are shown in Fig. 3 as a reference. The stress-strain curves of samples by CSR and LLR are shown in Figs. 4 and 5, respectively. Compressive strengths of these 21 specimens are summarized in Table 4.

Table 2 Geometrical parameters of carbon-nanotube shaped reinforcement

CSR	Height, H (mm)	Diameter, Φ (mm)	Volume, V (mm^3)	Rod length, L (mm)	Rod diameter, d (mm)	Node diameter, D (mm)
C10	190	90	27219	15.50	3.0	6.0
C12	190	90	34420	13.45	3.0	6.0
C14	190	90	46773	11.70	3.0	6.0

Table 3 Geometrical parameters of traditional latitude and longitude reinforcement

LLR	Height, H (mm)	Diameter, Φ (mm)	Volume, V (mm^3)	Vertical rod, L_1 (mm)	Transverse rod, L_2 (mm)	Rod diameter, d (mm)
P10	190	90	29977	23.75	28.27	3.0
P12	190	90	34073	21.11	23.56	3.0
P14	190	90	39941	17.27	20.20	3.0

Table 4 Compressive strength

Reinforcement	Sample	Compressive strength (MPa)	Average compressive strength (MPa)
Without reinforcement	N-1	2.85	2.56
	N-2	2.40	
	N-3	2.44	
CSR	C10-1	3.90	4.09
	C10-2	4.34	
	C10-3	4.03	
	C12-1	4.62	4.76
	C12-2	4.78	
	C12-3	4.87	
	C14-1	5.11	5.35
	C14-2	5.31	
	C14-3	5.64	
LLR	P10-1	3.17	3.18
	P10-2	3.45	
	P10-3	2.93	
	P12-1	3.51	3.76
	P12-2	3.97	
	P12-3	3.80	
	P14-1	4.63	4.32
	P14-2	4.28	
	P14-3	4.04	

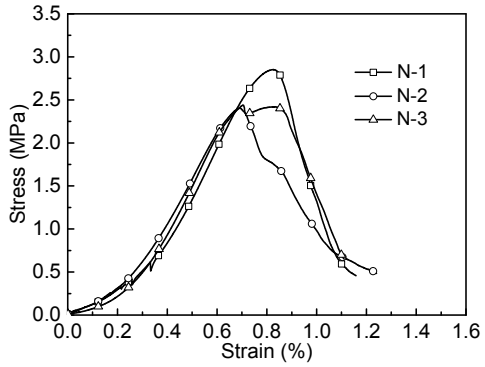

Fig. 3 Stress-strain curves of concrete without reinforcement

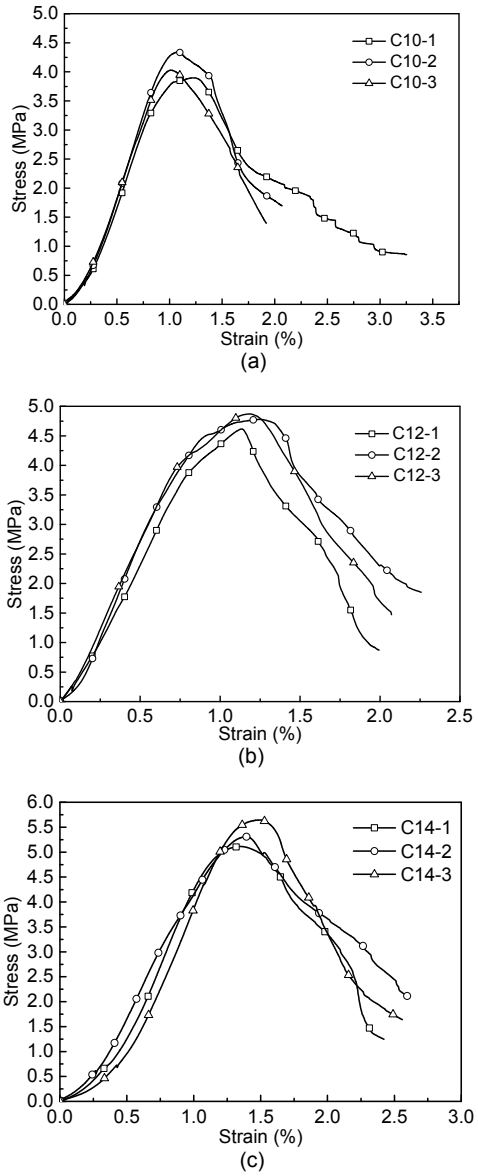

Fig. 4 Stress-strain curves of concrete by CSR
(a) C10; (b) C12; (c) C14

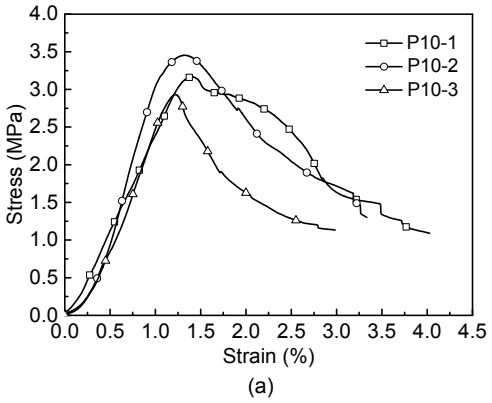

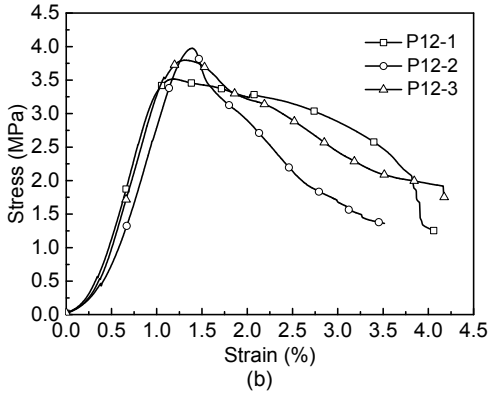

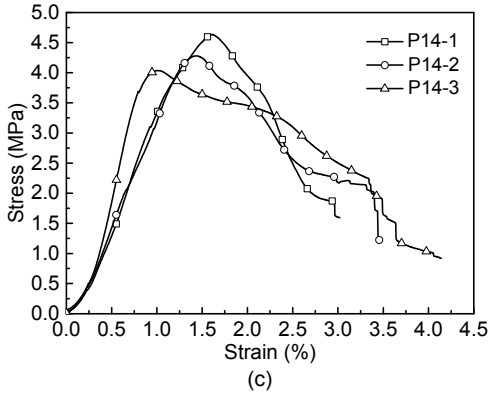

Fig. 5 Stress-strain curves of concrete by traditional LLR
(a) P10; (b) P12; (c) P14

From Table 4, it can be seen that each group of reinforced concrete has three compressive strengths, and the difference between the maximum and minimum is smaller than 15%. Therefore, the arithmetic average value of the three compressive strengths was taken as the average value of the compressive strength of the reinforced concrete according to the standard for the test method of basic properties of construction mortar (MOC, 2009).

3.2 Compressive strength

The stress-strain relationships for the specimens without reinforcement by CSR and LLR were averaged and compared in Fig. 6. Table 4 summarizes the compression strengths.

It can be seen from Table 4 and Fig. 6 that the peak strength of specimens without reinforcement is around 2.56 MPa. The peak strengths of specimens with different amounts of CSR are 4.09 MPa, 4.76 MPa, and 5.35 MPa, respectively. Compared with the unreinforced specimens, the strengths of specimens reinforced with C10, C12, and C14 increase by 59.77%, 85.94%, and 108.98%, respectively. The strengths of specimens reinforced by P10, P12, and P14 are 3.18 MPa, 3.76 MPa, and 4.32 MPa, which are increases of 24.22%, 46.88%, and 68.75%, respectively. From these comparisons, CSR is seen to increase the strength more significantly than the traditional LLR.

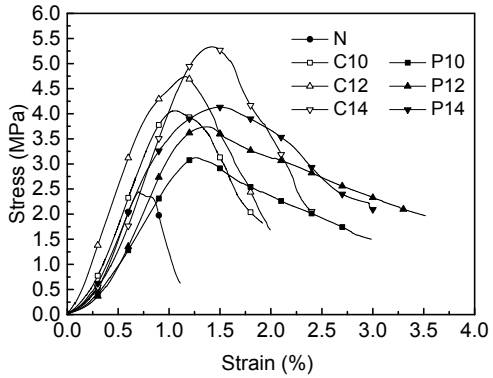

Fig. 6 Stress-strain curves of all specimens

3.3 Strain at peak stress

The strain at peak stress denotes the point when the material loses loading capacity. It is the initial point of sharply descending portion on the stress-strain curve. Table 5 shows the strain at the peak stress for the specimens. From Table 5, the strain at peak stress constantly increases with the increase in reinforcement ratio. The strain at peak stress of unreinforced specimens is 0.806%. The strains at peak stress of specimens reinforced by C10, C12, and C14 are 1.056%, 1.162%, and 1.426%, respectively. These are increases of 31.02%, 44.17%, and 76.92% compared to the unreinforced specimen. The strains at peak stress of specimens reinforced by P10, P12, and P14 are 1.261%, 1.372%, and 1.504% with respective percentage increases of 56.45%, 70.22%, and 86.60%. Both CSR and LLR improve the strain performance at peak strength substantially.

Table 5 Strain at peak stress

Reinforcement	Sample	Strain at peak stress (%)
Without reinforcement	N	0.806
CSR	C10	1.056
	C12	1.162
	C14	1.426
LLR	P10	1.261
	P12	1.372
	P14	1.504

3.4 Failure modes

Under compression loading, a crack first appeared at the end of the sample. This crack continued to expand and other cracks parallel to the first crack appeared. With further increase of the load, one of these cracks expanded to be the main crack in the vertical direction. When reinforced structures were damaged, part of the concrete covers spalled off with a distinctly audible cracking sound.

Specimens without reinforcement exhibit typical shear failure as characterized by a penetrating crack in the specimens and the failed specimens are divided into several parts as shown in Fig. 7. When specimens are reinforced with P10 and P12, a main crack appears along which the reinforced specimen fails as shown in Figs. 8 and 9. It can be interpreted as reinforcement

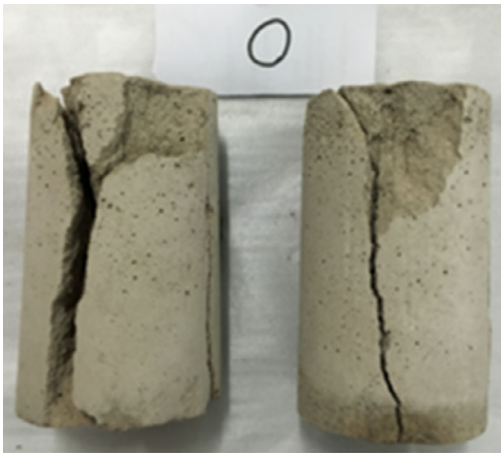

Fig. 7 Failure mode of specimens without reinforcement

improving the strength although it does not change the failure mode from that of the unreinforced specimen. On the other hand, the failure mode changes from global failure to partial failure in the specimens reinforced by P14 in Fig. 10. In view of their narrower width and shorter length compared to the specimens reinforced by P10 and P12 cracks are not so severe and a main crack does not appear. It does not run through the whole specimen to break it up as shown in Fig. 10. The dense reinforcement stops the crack from propagating throughout the whole specimen.

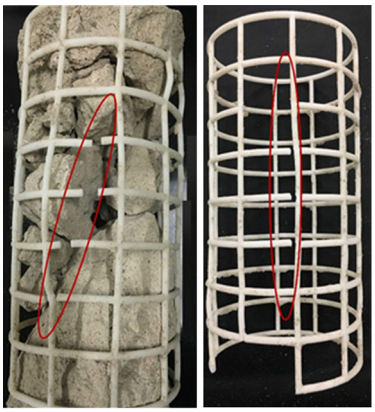

Fig. 8 Failure mode of specimens reinforced with P10

Fig. 9 Failure mode of specimens reinforced with P12

Fig. 10 Failure mode of specimens reinforced with P14

The damage patterns of the specimens reinforced by C10 are similar to those of the specimens reinforced by P10 and P12. There is a main crack running through the overall specimens and thus the reinforced specimens fail along the crack as shown in Fig. 11. The failure mode of specimens reinforced by C12 has both the features of global failure and partial failure. It can be seen in Fig. 12 that the specimen has a main crack running across the top to the bottom and the crack is wider in the middle. In addition, the concrete is crushed and the rods are broken at the top of the specimen. However, the failure mode is conspicuously changed from global failure to partial failure when the specimens are reinforced by C14 (Fig. 13).

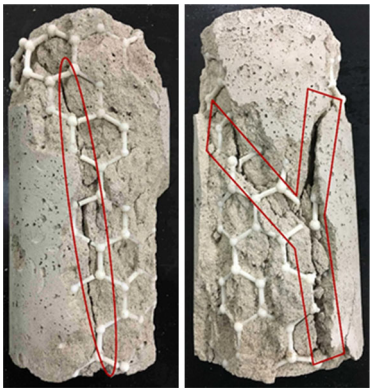

Fig. 11 Failure mode of specimens reinforced with C10

Fig. 12 Failure mode of specimens reinforced with C12

Comparing the failure modes of the specimens reinforced by different reinforcement ratios and

reinforcement types, it is observed from Figs. 7 to 13 that the failure mode switches from global failure to transient global-partial failure and then to partial failure as the reinforcement ratio increases. The specimens reinforced by P14 are damaged by a mixed mode of global failure and partial failure. For the specimens with CSR, the feature of partial failure appears when the specimens are reinforced by C12. The samples are damaged in the complete partial failure mode when the specimens are reinforced by C14.

It is seen from Figs. 6 to 13 that CSR shows improvements both in failure mode as well as in strength compared to the traditional LLR.

Fig. 13 Failure mode of specimens reinforced with C14

4 Conclusions

The present study investigates the uniaxial compression behavior of concrete specimens with different 3D-printed reinforcements. The present study contributes to providing a reference for the design standard for the application of 3D-printing in civil engineering. The following conclusions are drawn from the analysis of the physical compression tests.

1. The mechanical properties of specimens with reinforcement are much better than those of specimens without reinforcement. The strength and toughness of specimens with reinforcement increase constantly with the increase of the reinforcement ratio in the appropriate reinforcement ratio range.

2. The strength of specimens reinforced by CSR is greater than that of specimens reinforced by traditional LLR when the reinforcement ratio is similar.

3. The strains at peak stress for both types of reinforcement are barely influenced.

Currently, 3D-printing technology still has limitations, such as its inconvenience for practical engineering in the field. Future research will be conducted to overcome these demerits, e.g. through the provision of a 3D-printing machine suitable for practical engineering, an economic 3D-printing material, and the creation of design standards for the application of 3D-printing in civil engineering.

Contributors

Li-feng FAN conducted the investigation process. Li-juan WANG revised and edited the final version. Guo-wei MA formulated the overarching research goals and aims. Peng-fei LI took the responsibility for the research activity planning and execution. Ming-jie XIA wrote the first draft of the manuscript.

Conflict of interest

Li-feng FAN, Li-juan WANG, Guo-wei MA, Peng-fei LI, and Ming-jie XIA declare that they have no conflict of interest.

References

Ahmed SFU, Maalej M, 2009. Tensile strain hardening behaviour of hybrid steel-polyethylene fibre reinforced cementitious composites. *Construction and Building Materials*, 23(1):96-106. https://doi.org/10.1016/j.conbuildmat.2008.01.009

Ajayan PM, 1999. Nanotubes from carbon. *Chemical Reviews*, 99(7):1787-1800. https://doi.org/10.1021/cr970102g

Carballosa P, García Calvo JG, Revuelta D, et al., 2015. Influence of cement and expansive additive types in the performance of self-stressing and self-compacting concretes for structural elements. *Construction and Building Materials*, 93:223-229. https://doi.org/10.1016/j.conbuildmat.2015.05.113

Cesaretti G, Dini E, de Kestelier X, et al., 2014. Building components for an outpost on the Lunar soil by means of a novel 3D printing technology. *Acta Astronautica*, 93:430-450. https://doi.org/10.1016/j.actaastro.2013.07.034

Chen SJ, Duan WH, Li ZJ, et al., 2015. New approach for characterisation of mechanical properties of cement paste at micrometre scale. *Materials & Design*, 87:992-995. https://doi.org/10.1016/j.matdes.2015.08.101

Chi Y, Xu LH, Zhang YY, 2014. Experimental study on hybrid fiber-reinforced concrete subjected to uniaxial compression. *Journal of Materials in Civil Engineering*, 26(2):211-218. https://doi.org/10.1061/(ASCE)MT.1943-5533.0000764

Chuah S, Duan WH, Pan Z, et al., 2016. The properties of fly ash based geopolymer mortars made with dune sand.

Materials & Design, 92:571-578. https://doi.org/10.1016/j.matdes.2015.12.070

Dias DP, Thaumaturgo C, 2005. Fracture toughness of geopolymeric concretes reinforced with basalt fibers. *Cement and Concrete Composites*, 27(1):49-54. https://doi.org/10.1016/j.cemconcomp.2004.02.044

Fan LF, Wu ZJ, Wan Z, et al., 2017. Experimental investigation of thermal effects on dynamic behavior of granite. *Applied Thermal Engineering*, 125:94-103. https://doi.org/10.1016/j.applthermaleng.2017.07.007

Jiang JY, Sun W, Zhang YS, et al., 2008. Cracking resistance performance of super vertical-distance pumped SFRC. *Frontiers of Architecture and Civil Engineering in China*, 2(2):179-183. https://doi.org/10.1007/s11709-008-0018-6

Jiang YJ, Fan LF, 2013. An investigation of mechanical behavior of cement-stabilized crushed rock material using different compaction methods. *Construction and Building Materials*, 48:508-515. https://doi.org/10.1016/j.conbuildmat.2013.07.017

Jiang YJ, Fan LF, 2015. An experimental investigation of optimal asphalt-aggregate ratio for different compaction methods. *Construction and Building Materials*, 91:111-115. https://doi.org/10.1016/j.conbuildmat.2015.05.054

Le TT, Austin SA, Lim S, et al., 2012. Hardened properties of high-performance printing concrete. *Cement and Concrete Research*, 42(3):558-566. https://doi.org/10.1016/j.cemconres.2011.12.003

Lee YH, Kim SG, Tománek D, 1997. Catalytic growth of single-wall carbon nanotubes: an ab initio study. *Physical Review Letters*, 78(12):2393-2396. https://doi.org/10.1103/PhysRevLett.78.2393

Lin XS, Zhang YX, Hazell PJ, 2014. Modelling the response of reinforced concrete panels under blast loading. *Materials & Design*, 56:620-628. https://doi.org/10.1016/j.matdes.2013.11.069

Lu DC, Zhou X, Du XL, et al., 2019. A 3D fractional elastoplastic constitutive model for concrete material. *International Journal of Solids and Structures*, 165:160-175. https://doi.org/10.1016/j.ijsolstr.2019.02.004

Micelli F, Nanni A, 2004. Durability of FRP rods for concrete structures. *Construction and Building Materials*, 18(7):491-503. https://doi.org/10.1016/j.conbuildmat.2004.04.012

Michalski MH, Ross JS, 2014. The shape of things to come: 3D printing in medicine. *JAMA*, 312(21):2213-2214. https://doi.org/10.1001/jama.2014.9542

MOC (Ministry of Construction of the People's Republic of China), 2003. Standard for Test Method of Mechanical Properties on Ordinary Concrete, GB/T 50081-2002. National Standards of the People's Republic of China (in Chinese).

MOC (Ministry of Construction of the People's Republic of China), 2009. Standard for Test Method of Basic Properties of Construction Mortar, JGJ/T 70-2009. Industry Standards of the People's Republic of China (in Chinese).

MOHURD (Ministry of Housing and Urban-Rural Development of the People's Republic of China), 2010a. Code for Design of Concrete Structures, GB 50010-2010. National Standards of the People's Republic of China (in Chinese).

MOHURD (Ministry of Housing and Urban-Rural Development of the People's Republic of China), 2010b. Specification for Mix Proportion Design of Masonry Mortar, JGJ/T 98-2010. Industry Standards of the People's Republic of China (in Chinese).

Ouyang XP, Qiu XQ, Chen P, 2006. Physicochemical characterization of calcium lignosulfonate—a potentially useful water reducer. *Colloids and Surfaces A: Physicochemical and Engineering Aspects*, 282-283:489-497. https://doi.org/10.1016/j.colsurfa.2005.12.020

Pegna J, 1997. Exploratory investigation of solid freeform construction. *Automation in Construction*, 5(5):427-437. https://doi.org/10.1016/S0926-5805(96)00166-5

Pendhari SS, Kant T, Desai YM, 2008. Application of polymer composites in civil construction: a general review. *Composite Structures*, 84(2):114-124. https://doi.org/10.1016/j.compstruct.2007.06.007

Salvetat JP, Bonard JM, Thomson NH, et al., 1999. Mechanical properties of carbon nanotubes. *Applied Physics A*, 69(3):255-260. https://doi.org/10.1007/s003390050999

Sanz-Izquierdo B, Parker EA, 2013. 3D printing technique for fabrication of frequency selective structures for built environment. *Electronics Letters*, 49(18):1117-1118. https://doi.org/10.1049/el.2013.2256

Treacy MMJ, Ebbesen TW, Gibson JM, 1996. Exceptionally high Young's modulus observed for individual carbon nanotubes. *Nature*, 381(6584):678-680. https://doi.org/10.1038/381678a0

Tsonos AG, 2008. Effectiveness of CFRP-jackets and RC-jackets in post-earthquake and pre-earthquake retrofitting of beam-column subassemblages. *Engineering Structures*, 30(3):777-793. https://doi.org/10.1016/j.engstruct.2007.05.008

Walters P, Davies K, 2010. 3D printing for artists: research and creative practice. *Rapport: Journal of the Norwegian Print Association*, 1:12-15.

Wang GS, Lu DC, Du XL, et al., 2018. A true 3D frictional hardening elastoplastic constitutive model of concrete based on a unified hardening/softening function. *Journal of the Mechanics and Physics of Solids*, 119:250-273. https://doi.org/10.1016/j.jmps.2018.06.019

Wight RG, Green MF, Erki MA, 2001. Prestressed FRP sheets for poststrengthening reinforced concrete beams. *Journal of Composites for Construction*, 5(4):214-220. https://doi.org/10.1061/(ASCE)1090-0268(2001)5:4(214)

Wong EW, Sheehan PE, Lieber CM, 1997. Nanobeam mechanics: elasticity, strength, and toughness of nanorods and nanotubes. *Science*, 277(5334):1971-1975. https://doi.org/10.1126/science.277.5334.1971

Wu W, Zhang WD, Ma GW, 2010a. Mechanical properties of

copper slag reinforced concrete under dynamic compression. *Construction and Building Materials*, 24(6):910-917.
https://doi.org/10.1016/j.conbuildmat.2009.12.001

Wu W, Zhang WD, Ma GW, 2010b. Optimum content of copper slag as a fine aggregate in high strength concrete. *Materials & Design*, 31(6):2878-2883.
https://doi.org/10.1016/j.matdes.2009.12.037

Zhang YX, Zhu Y, 2010. A new shear-flexible FRP-reinforced concrete slab element. *Composite Structures*, 92(3):730-735.
https://doi.org/10.1016/j.compstruct.2009.09.013

Introducing Editorial Board Member:

Prof. Li-feng FAN has been a member of the editorial board of *Journal of Zhejiang University-SCIENCE A (Applied Physics & Engineering)* since 2018. He is a professor of Beijing University of Technology, China. Prof. FAN received his bachelor and master degrees from Xi'an Jiaotong University, China in 2003 and 2006, respectively, and PhD degree from Nanyang Technology University, Singapore in 2012.

Prof. FAN was honored as "Young Yangtze River Scholar" (Ministry of Education) and "Great Wall Scholar" (Beijing) in 2017. He is a committee member of "Rock Dynamics Commission" and "Rock Mechanics Educational Commission" of Chinese Society for Rock Mechanics & Engineering. He was also the co-chair of the 14th International Conference on Analysis of Discontinuous Deformation.

Until now, Prof. FAN has led three National Natural Science Foundations of China and participated in a few other national projects. He has published more than 50 SCI papers (37 papers as first or corresponding author). His field of research includes rock dynamics, seismic wave propagation, and 3D printing for civil engineering.

中文概要

题　目： **3D 打印仿碳纳米管加筋混凝土单轴受压力学性能研究**

目　的： 研究 3D 打印仿碳纳米管加筋结构对混凝土单轴受压力学性能的加固机制。

创新点： 提出一种采用仿碳纳米管加筋结构对混凝土进行加固的方法。

方　法： 1. 以韧性树脂为材料，采用光固化 3D 打印技术分别制作疏密度为每层 10 个单元、12 个单元和 14 个单元的仿碳纳米管加筋结构和传统纵横加筋结构。2. 将配制的 M2.5 水泥砂浆作为填充材料，制备直径为 100 mm、高为 200 mm 的圆柱型单轴压缩试件。3. 以相同尺寸内部无加筋的素混凝土试件作为参考进行抗压试验。

结　论： 1. 与素混凝土相比，当试件采用每层 10 个单元、12 个单元和 14 个单元的仿碳纳米管加筋结构时，混凝土试件抗压强度分别提高 59.77%、85.94% 和 108.98%。2. 当试件采用每层 10 个单元、12 个单元和 14 个单元的传统纵横加筋结构时，混凝土试件抗压强度分别提高 24.22%、46.88%和 68.75%。3. 仿碳纳米管加筋结构对混凝土的加固效果明显优于传统纵横加筋结构。4. 仿碳纳米管加筋后试件的破坏形式随着加筋密度的增加由整体破坏转变为局部破坏。

关键词： 3D 打印；仿碳纳米管加筋；纵横加筋；混凝土加固